J. Fluid Mech. (1978), *vol.* 86, *part* 1, *pp.* 1–14
Printed in Great Britain

Laminar throughflow between closely spaced rotating disks

By A. Z. SZERI AND M. L. ADAMS†

Department of Mechanical Engineering, University of Pittsburgh, Pennsylvania 15261

(Received 18 November 1976 and in revised form 10 October 1977)

Laminar throughflow between finite parallel disks, one stationary and the other rotating, can be characterized by four dimensionless parameters in the general case. But, if the ratio of disk spacing to disk radius is small, an approximate definition of the flow may be made with reference to a single parameter, the Ekman number. The equations of motion and the equation of continuity in this 'thin-film' approximation are reduced here to an initial-value problem for nonlinear ordinary differential equations, by a Galerkin-type procedure. Hamming's modified predictor–corrector method is employed subsequently to solve for the stream functions. Radial pressure profiles of this solution are compared with published experimental data. The calculated results may be applied to the design of hydrostatic bearings and face seals.

1. Introduction

The laminar throughflow which occurs between parallel disks when one disk is rotated and the other is stationary while a line source is placed coincident with the axis of rotation may be applied to the design of hydrostatic bearings, face seals, clutch plates and rotating heat exchangers. When the disks are of finite radius and the film is thick, the flow can be characterized in terms of four dimensionless parameters and two sets of boundary conditions, which are prescribed at some starting radius $r_1 > 0$ and at the disk radius r_2, respectively. If, however, the ratio s/r_2 of disk separation to disk radius is small and if attention is limited to some annular region $r_1 < r < r_B$, where r_B is the position of incipient backflow, the flow is adequately described by a single dimensionless parameter, the Ekman number. As the problem becomes parabolic under this 'thin-film' approximation, boundary conditions may no longer be prescribed at the disk radius r_2. Furthermore, the precise nature of the boundary (now initial) conditions that are to be prescribed at the starting radius $r_1 > 0$ becomes less important, as these conditions are washed out within a short distance downstream from r_1. Their significance is retained only as it relates to the number of terms that must be included in our series solution to give a specified accuracy. It was found that convergence of the pressure is fastest if the initial conditions are given by the creeping-flow solution. It is emphasized, however, that identical velocity profiles are obtained with different initial conditions (Szeri & Adams 1976).

The problem of laminar throughflow between closely spaced disks, either stationary or rotating, has been discussed extensively in the literature, both experimentally and theoretically. When the two disks are stationary and fluid inertia is neglected, theory

† Present address: Department of Mechanical Engineering, University of Akron, Ohio.

predicts that a logarithmic pressure drop is required by viscous dissipation. Experiments performed at low flow rates verify this theoretical result (Coombs & Dowson 1965). If the throughflow Reynolds number (defined by $R_Q = Q/2\pi\nu s$, where Q is the flow rate) is now increased, convective inertia gains importance. Its effect is to increase the pressure in the radial direction, rapidly at small radii and more moderately at large radii. At small values of the dimensionless radius defined by $\rho = r/sR_Q^{\frac{1}{2}}$, convective inertia effects outweigh viscous dissipation, whereas at large ρ they only slightly modify the creeping-flow solution. To account for the effect of convective inertia Livesey (1960) argued that departure from parallel flow must be slight even at large flow rates. Retaining $u\partial u/\partial r$ as the only significant inertia term, where u is the similar profile of the creeping-flow solution, he found that

$$\frac{d\bar{p}}{d\rho} = -\frac{12}{\rho} + \frac{2K}{\rho^3}.$$

Here $\bar{p} = ps^2/\mu\nu R_Q$ is the dimensionless pressure. The value of K was given by Livesey as 0·6. By assuming a slight departure from the parabolic velocity profile of creeping flow, Moller (1963) found the value $K = 0{\cdot}72$. Jackson & Symmons (1965*a*) followed the earlier work of Hunt & Torbe (1962) and expanded the radial velocity in powers of r_2/r, the coefficients of this series being functions of the normal co-ordinate. Jackson & Symmons calculated $K = 0{\cdot}77143$. A small perturbation of the creeping-flow solution led Savage (1964) to identical results.

When one of the disks is rotating, there is further distortion of the creeping-flow profile due to centrifugal inertia. That this distortion can be large enough to destroy the load capacity of a hydrostatic bearing was convincingly demonstrated by Osterle & Hughes (1957/8). The solution was based on the assumptions of negligible convective inertia and a rotational inertia calculated from a linear circumferential velocity. Their radial pressure gradient can be represented in the form

$$\frac{d\bar{P}}{d\rho} = -\frac{12}{\rho} + \frac{3\rho}{10E^2},$$

where $E = \nu/s^2\omega$ is the Ekman number and ω is the disk's angular velocity. Dowson (1961) applied identical considerations to a hydrostatic step bearing geometry. His results are in agreement with the findings of Osterle & Hughes.

Experimental data are given by Moller (1963) and by Jackson & Symmons (1965*b*) for stationary disks. Throughflow between a stationary and a rotating disk was investigated experimentally by Coombs & Dowson (1965), Makay (1967) and Nirmel (1970).

2. Analysis

Two parallel disks of radius r_2, one stationary and the other rotating at a constant rate ω, are located at $z = 0$ and $z = s$, respectively, in a cylindrical co-ordinate system (r, θ, z). Relative to this co-ordinate system, if rotational symmetry is postulated, the equations of motion and continuity are as follows:

$$u\frac{\partial u}{\partial r} - \frac{v^2}{r} + w\frac{\partial u}{\partial z} = \nu\left(\nabla^2 u - \frac{u}{r^2}\right) - \frac{1}{\rho}\frac{\partial p}{\partial r}, \tag{1a}$$

$$\frac{u}{r}\frac{\partial}{\partial r}(rv)+w\frac{\partial v}{\partial z}=\nu\left(\nabla^2 v-\frac{v}{r^2}\right), \tag{1b}$$

$$u\frac{\partial w}{\partial r}+w\frac{\partial w}{\partial z}=\nu\nabla^2 w-\frac{1}{\rho}\frac{\partial p}{\partial z}, \tag{1c}$$

$$\frac{\partial}{\partial r}(ru)+\frac{\partial}{\partial z}(rw)=0 \tag{1d}$$

in $$0<r_1<r<r_2, \quad 0<z<s.$$

The equation of continuity is identically satisfied by taking

$$u=r^{-1}\partial\Psi/\partial z, \quad w=-r^{-1}\partial\Psi/\partial r, \tag{2}$$

and henceforth the equations of motion are written in terms of the stream function Ψ. If, in addition, the pressure is eliminated from the first and the third momentum equations then the system of equations (1) can be replaced by the following two equations:

$$\frac{\partial\Psi}{\partial z}\frac{\partial(D^2\Psi)}{\partial r}-\frac{\partial\Psi}{\partial r}\frac{\partial(D^2\Psi)}{\partial z}-\frac{2v}{r}\frac{\partial v}{\partial r}=\nu\left(r^3D^2+4\frac{\partial}{\partial r}\right)D^2\Psi, \tag{3}$$

$$\frac{\partial\Psi}{\partial z}\frac{\partial(rv)}{\partial r}-\frac{\partial\Psi}{\partial r}\frac{\partial(rv)}{\partial z}=\nu r^3D^2(rv), \tag{4}$$

where the operator is defined by

$$D^2=\frac{1}{r^2}\left(\nabla^2-\frac{2}{r}\frac{\partial}{\partial r}\right).$$

The boundary conditions on Ψ and v at the disks are dictated by no slip and by mass conservation:

$$\partial\Psi/\partial r=\partial\Psi/\partial z=v=0 \quad \text{at} \quad z=0, \tag{5a}$$

$$\partial\Psi/\partial r=\partial\Psi/\partial z=0, \quad v=r\omega \quad \text{at} \quad z=s, \tag{5b}$$

$$\Psi(r,s)-\Psi(r,0)=Q/2\pi, \tag{5c}$$

where

$$Q=2\pi r\int_0^s u(r,z)\,dz$$

is the net rate of flow across an arbitrary cylinder $r=$ constant.

In addition to (5) we specify the following conditions at some $r=r_1$ and at $r=r_2$:

$$\Psi=\phi(z), \quad v=v_1(z) \quad \text{at} \quad r=r_1>0, \tag{6a}$$

$$\Psi=\phi(z), \quad v=v_2(z) \quad \text{at} \quad r=r_2. \tag{6b}$$

Let the dimensionless quantities ζ, ρ, $\bar{\Psi}$ and $\bar{\Omega}$ be defined by

$$z=k_1\zeta, \quad r=k_2\rho, \quad \Psi=k_3\bar{\Psi}, \quad v=k_2k_4\rho\bar{\Omega}. \tag{7}$$

Substitution of (7) into (3)–(6) yields the equations

$$\frac{\partial\bar{\Psi}}{\partial\zeta}\frac{\partial(\bar{D}^2\bar{\Psi})}{\partial\rho}-\frac{\partial\bar{\Psi}}{\partial\rho}\frac{\partial(\bar{D}^2\bar{\Psi})}{\partial\zeta}-\left(\frac{k_2^3k_4}{k_3}\right)^2 2\bar{\Omega}\frac{\partial(\rho\bar{\Omega})}{\partial\zeta}=\frac{\nu k_1}{k_3}\left(\rho^3\bar{D}^2+4\frac{\partial}{\partial\rho}\right)(\bar{D}^2\bar{\Psi}), \tag{8}$$

$$\frac{\partial\Psi}{\partial\zeta}\frac{\partial(\rho^2\bar{\Omega})}{\partial\rho}-\frac{\partial\bar{\Psi}}{\partial\rho}\frac{\partial(\rho^2\bar{\Omega})}{\partial\zeta}=\frac{\nu k_1}{k_3}\rho^3\bar{D}^2(\rho^2\bar{\Omega}) \tag{9}$$

and the boundary conditions

$$\partial\bar{\Psi}/\partial\rho = \partial\bar{\Psi}/\partial\zeta = \bar{\Omega} = 0 \quad \text{at} \quad \zeta = 0, \tag{10a}$$

$$\partial\bar{\Psi}/\partial\rho = \partial\bar{\Psi}/\partial\zeta = 0, \quad \bar{\Omega} = 1 \quad \text{at} \quad \zeta = 1, \tag{10b}$$

$$\bar{\Psi} = \bar{\phi}(\zeta), \quad \bar{\Omega} = \bar{\theta}(\zeta) \quad \text{at} \quad \rho = \rho_1, \rho_2, \tag{10c}$$

$$\bar{\Psi}(\rho, 1) - \bar{\Psi}(\rho, 0) = Q/2\pi k_3. \tag{10d}$$

Equations (8)–(10) represent our mathematical model of the flow in the general case. This model is dependent on four dimensionless parameters.

The number of essential flow parameters can be reduced if the gap between the disks is narrow, i.e. if $s/r_2 \ll 1$, for then the radial variation of the shear stress may be ignored and we have the approximation

$$\bar{D}^2 \simeq \frac{1}{\rho^2}\frac{\partial^2}{\partial\zeta^2}, \quad \frac{s}{r_2} \ll 1. \tag{11}$$

For this thin-film case it is expedient to choose the normalizing constants in (7) as

$$k_1 = s, \quad k_2 = sR_Q^{\frac{1}{2}}, \quad k_3 = \nu s R_Q, \quad k_4 = \omega, \tag{12}$$

where $R_Q = Q/2\pi\nu s$ is the throughflow Reynolds number.

Substitution of (11) and (12) reduces (8) and (9) to the form

$$\frac{\partial\bar{\Psi}}{\partial\zeta}\frac{\partial}{\partial\rho}\left(\frac{1}{\rho^2}\frac{\partial^2\bar{\Psi}}{\partial\zeta^2}\right) - \frac{\partial\bar{\Psi}}{\partial\rho}\frac{\partial}{\partial\zeta}\left(\frac{1}{\rho^2}\frac{\partial^2\bar{\Psi}}{\partial\zeta^2}\right) - \frac{1}{E^2}\frac{\partial(\rho\bar{\Omega}^2)}{\partial\zeta} = \frac{1}{\rho}\frac{\partial^4\bar{\Psi}}{\partial\zeta^4}, \tag{13}$$

$$\frac{\partial\bar{\Psi}}{\partial\zeta}\frac{\partial(\rho^2\bar{\Omega})}{\partial\rho} - \frac{\partial\bar{\Psi}}{\partial\rho}\frac{\partial(\rho^2\bar{\Omega})}{\partial\zeta} = \rho\frac{\partial^2(\rho^2\bar{\Omega})}{\partial\zeta^2}. \tag{14}$$

The simplification of (8) and (9) that is achieved by the choice of the constants (12) and the approximation in (11) is considerable. Equations (13) and (14) are both of only first order in ρ and, in addition, the flow is now characterized by a single dimensionless parameter, the Ekman number $E = \nu/s^2\omega$.

It is true that two additional parameters ρ_1 and ρ_2 have formally been retained in the boundary conditions even though the approximation (11) has been made, but (13) and (14) are now parabolic in ρ with the consequences that (*a*) boundary conditions may be prescribed at only a single (upstream) ρ position and (*b*) just a short distance downstream from that ρ boundary the family of flows with a given Ekman number but various initial conditions have identical dimensionless velocity profiles. Thus the two parameters ρ_1 and ρ_2 lose their significance as defining parameters when solving for thin films, leaving the Ekman number as the single parameter of the model.

The partial differential equations (13) and (14) are first reduced to two systems of ordinary differential equations. To this end two complete sets of functions $\{F_n(\zeta)\}$ and $\{G_n(\zeta)\}$ are considered whose elements have continuous derivatives to the right order in $0 < \zeta < 1$ and vanish, together with F_n', at both $\zeta = 0$ and $\zeta = 1$. It is assumed that the Nth approximations $\bar{\Psi}_N$ and $\bar{\Omega}_N$ to $\bar{\Psi}$ and $\bar{\Omega}$, respectively, can be expanded in the series

$$\bar{\Psi}_N = \bar{\phi}(\zeta) + \sum_{n=1}^{N} F_n(\zeta) f_n(\rho), \tag{15a}$$

$$\bar{\Omega}_N = \bar{\theta}(\zeta) + \sum_{n=1}^{N} G_n(\zeta) g_n(\rho), \tag{15b}$$

with suitable conditions on $\bar{\phi}(\zeta)$ and $\bar{\theta}(\zeta)$ at $\zeta = 0,\ 1$ and on $f_n(\rho)$ and $g_n(\rho)$ at $\rho = \rho_1$.

Applying the usual arguments of the Galerkin–Kantorovich method, (13) and (14) are replaced by two sets of nonlinear ordinary differential equations:

$$-\frac{2}{\rho}A_k^{(1)} - \frac{2\rho^3}{\pi^2 E^2}A_k^{(11)} - \pi\rho A_k^{(9)} + \sum_n^N \left\{\left(-\frac{2}{\rho}A_{kn}^{(2)} - \pi\rho A_{kn}^{(10)}\right)f_n + (A_{kn}^{(4)} - A_{kn}^{(5)})f_n' - \frac{2\rho^3}{\pi^2 E^2}A_{kn}^{(7)}g_n\right\} + \sum_{n,j}^N \left\{A_{knj}^{(3)}f_n\left(f_j' - \frac{2}{\rho}f_j\right) - A_{knj}^{(6)}f_n'f_j - \frac{2\rho^3}{\pi^2 E^2}A_{knj}^{(8)}g_n g_j\right\} = 0, \quad k = 1, 2, 3, \ldots, N, \tag{16}$$

and

$$\frac{2}{\rho}B_k^{(1)} - \pi\rho B_k^{(7)} + \sum_n^N \left\{\frac{2}{\rho}B_{kn}^{(2)}f_n + \left(\frac{2}{\rho}B_{kn}^{(3)} - \pi\rho B_{kn}^{(8)}\right)g_n + B_{kn}^{(3)}g_n' - B_{kn}^{(5)}f_n'\right\} + \sum_{n,j}^N \left\{B_{knj}^{(4)}f_n\left(\frac{2}{\rho}g_j + g_j'\right) - B_{knj}^{(6)}f_n'g_j\right\} = 0, \quad k = 1, 2, 3, \ldots, N. \tag{17}$$

The coefficients $A_n^{(1)}$, $A_{kn}^{(2)}, \ldots, B_{knj}^{(8)}$ are defined in the appendix.

Selecting

$$\bar{\phi} = \zeta^2(3 - 2\zeta), \quad \bar{\theta} = \zeta, \tag{18a, b}$$

$$F_n(\zeta) = \cos\{(n-1)\pi\zeta\} - \cos\{(n+1)\pi\zeta\}, \tag{18c}$$

$$G_n(\zeta) = \sin(n\pi\zeta), \tag{18d}$$

$\bar{\Psi}_N$ and $\bar{\Omega}_N$ satisfy all the boundary conditions of the problem, provided that we require that

$$f_n(\rho_1) = 0, \quad g_n(\rho_1) = 0. \tag{19}$$

Note that (18) turns (15) into a perturbation of the creeping-flow solution. This represents an improvement, in the number of terms required for a given accuracy, over Szeri & Adams (1976).

Equations (16) and (17) together with conditions (19) define an initial-value problem. This initial-value problem was solved numerically, using Hamming's modified predictor–corrector method. Solutions were obtained over a wide range of the parameter E, using approximations up to and including $N = 8$. (For details see Adams 1977.)

Having found approximations to the true solutions $\bar{\Psi}$ and $\bar{\Omega}$, we are in a position to calculate the radial variation of the averaged pressure

$$P(\rho) = \frac{\mu\nu R_Q}{s^2}\bar{P}(\rho) = \frac{1}{s}\int_0^s p(r, z)\,dz. \tag{20}$$

From the first of the momentum equations (1) one obtains

$$\frac{d\bar{P}}{d\rho} = \frac{6}{5\rho^3} + \frac{\rho}{3E^2} - \frac{12}{\rho} + \sum_n \left\{\frac{96}{\pi^2\rho^2}X_n\left(f_n' - \frac{1}{\rho}f_n\right) - \frac{4\pi^2 n[(-1)^n + 1]}{\rho}f_n + \frac{\rho}{E^2}\left[\tfrac{1}{2}g_n^2 - 2\frac{(-1)^n}{\pi n}g_n\right]\right\} + \sum_{n,m} Y_{n,m}\left[\frac{\pi}{\rho^3}f_n f_m - \frac{2\pi}{\rho^2}f_n' f_m\right], \tag{21}$$

	$\Delta\bar{P}(\rho; 0{\cdot}78)$ at $E = 100$			$\Delta\bar{P}(\rho; 7{\cdot}0)$ at $E = 2{\cdot}9$	
ρ	$\rho_1 = 0{\cdot}1$	$\rho_1 = 0{\cdot}3$	ρ	$\rho_1 = 1{\cdot}0$	$\rho_1 = 3{\cdot}2$
0·10	−35·92	—	1·0	21·782	—
0·22	−9·02	—	2·0	14·046	—
0·30	0·23	4·83	3·2	8·626	8·617
0·38	3·74	4·45	3·3	8·272	8·264
0·46	3·86	3·91	3·4	7·930	7·923
0·54	3·04	3·04	4·0	6·077	6·072
0·62	2·03	2·03	5·0	3·580	3·578
0·70	1·00	1·00	6·0	1·604	1·603

TABLE 1. Effect of starting radius ρ_1 on pressure drop $\Delta\bar{P}$.

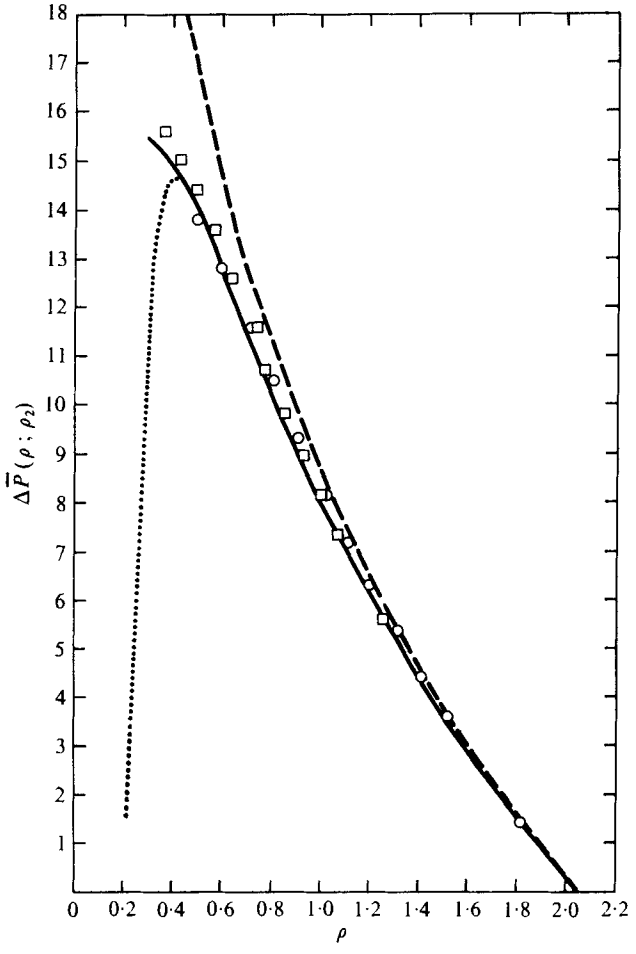

FIGURE 1. $\overline{\Delta P}(\rho;\rho_2)$ *vs.* ρ. Experimental data (Moller 1963): ○, $R_Q = 1{\cdot}08\times10^5$, $s = 3{\cdot}81\times10^{-2}$ cm; □, $R_Q = 5{\cdot}41\times10^4$, $s = 7{\cdot}62\times10^{-2}$ cm. Theory: – – –, creeping flow; ——, $\rho_1 = 0{\cdot}3$, present authors; ····, $\rho_1 = 0{\cdot}1$, present authors.

where

$$Y_{n,m} = \begin{cases} \pi(n^2+1) & \text{if} \quad n = m, \\ -\frac{1}{2}\pi(m \pm 1)^2 & \text{if} \quad n = m \pm 2, \\ 0 & \text{otherwise}, \end{cases}$$

$$X_n = n[1+(-1)^n]/(n^2-1)^2 \quad \text{if} \quad n \neq 1, \quad X_1 = 0.$$

It may be remarked here that in (21) the term $-12/\rho$ represents the contribution of creeping flow, the term $\rho/3E^2$ is directly comparable with the term $3\rho/10E^2$ of Osterle & Hughes (1957/8) for rotational inertia, and the term $6/5\rho^3$ corresponds to the convective-inertia term $2K/\rho^3$ of Livesey (1960). Then at any radial position r

$$P(r) = P(r_1) + (\mu\nu R_Q/s^2)\,\Delta\bar{P}(\rho;\rho_1), \tag{22}$$

where

$$\Delta\bar{P}(\rho;\rho_1) = \int_{\rho_1}^{\rho} \frac{d\bar{P}(\rho)}{d\rho}\,d\rho$$

is calculated from (21).

It is a premise of the present analysis that the initial conditions are washed out completely within a short distance, so that

$$\Delta\bar{P}(\rho_b;\rho_c) = \Delta\bar{P}(\rho_b;\rho_a) - \Delta\bar{P}(\rho_c;\rho_a), \quad \rho_a < \rho_b < \rho_c, \tag{23}$$

is independent of conditions (10) and is valid for all thin films without backflow at points sufficiently far removed from the 'inlet'. This is illustrated in table 1 and figure 1 for specific cases.

The definition

$$\Delta\bar{W}(\rho;\rho_1) = 2\pi \int_{\rho_1}^{\rho} \rho\,\Delta\bar{P}\,d\rho, \quad \Delta\bar{P}(\rho_1) = 0, \tag{24}$$

leads to the resultant fluid force W on either disk:

$$W(r;r_1)/\mu\nu R_Q^2 = \bar{W}(r;r_1) - \pi(\rho^2-\rho_1^2)\,\Delta\bar{P}(\rho;\rho_1). \tag{25}$$

The formula

$$\frac{W(r_2;r_1)}{\mu\nu R_Q^2} = \frac{W(r_i;r_1)}{\mu\nu R_Q^2} + \frac{W(r_2;r_i)}{\mu\nu R_Q^2} - \pi(\rho_i^2-\rho_1^2)\,\Delta\bar{P}(\rho_2;\rho_i), \quad r_1 < r_i < r_2, \tag{26}$$

is also useful in applications.

The torque coefficient C_M is defined by

$$C_M(\rho;\rho_1)_{R,S} = M(r;r_1)_{R,S}/s\mu\nu R_Q^2,$$

where the subscripts R and S refer to the rotating disk and the stationary disk, respectively. The torque coefficients have properties similar to those of $\Delta\bar{P}$ and are calculated from

$$\frac{2E}{\pi}(C_M)_R = \frac{1}{4}(\rho^4-\rho_1^4) + 4\pi \sum_n n(-1)^n \int_{\rho_1}^{\rho} \rho^3 g_n(\rho)\,d\rho \tag{27}$$

and

$$\frac{2E}{\pi}(C_M)_S = \frac{1}{4}(\rho^4-\rho_1^4) + 4\pi \sum_n n \int_{\rho_1}^{\rho} \rho^3 g_n(\rho)\,d\rho. \tag{28}$$

In these equations $\pi(\rho^4-\rho_1^4)/2E$ is the torque coefficient of the linear (unperturbed) circumferential velocity.

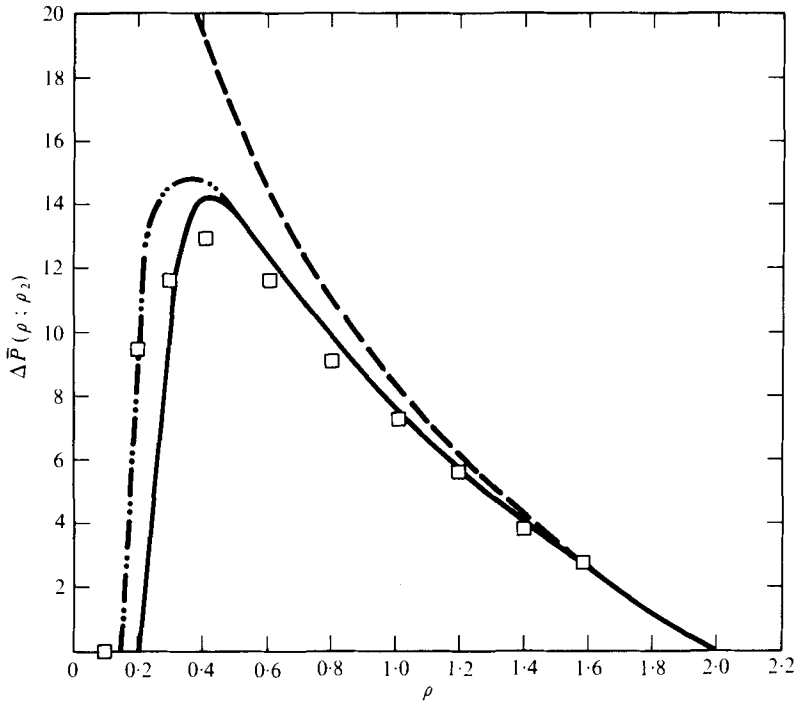

FIGURE 2. $\overline{\Delta P}(\rho;\rho_2)$ *vs.* ρ. □, experimental data, $R_Q = 8{\cdot}78 \times 10^3$, $s = 2{\cdot}54 \times 10^{-2}$ cm (Jackson & Symmons 1965*b*). Theory: –·–·–, Jackson & Symmons (1965*b*); – – –, creeping flow; ——, present authors.

3. Discussion

Results of the thin-film approximation are compared with published experimental data in two categories. In the first category of experiments both disks are stationary. Though the present solution calculates flows without swirl only in the limit $E \to \infty$, at $E = 100$ and $\rho < 4$ the ratio of rotational inertia to convective inertia is at most of order 10^{-3}. Thus solutions obtained under these conditions can, and will be, used to predict the flow between stationary disks. Figure 1 indicates that at large values of ρ the creeping-flow solution adequately describes flow with no swirl. But as ρ decreases, corresponding to an increase in flow rate with a fixed geometry, creeping flow seriously over-estimates the pressure drop. The experimental data in this figure were obtained with $0{\cdot}27 < \rho_1 < 0{\cdot}36$. Figure 1 also contains theoretical curves calculated with $\rho_1 = 0{\cdot}1$ and $\rho_1 = 0{\cdot}3$, respectively. In light of figure 1 our earlier statement that initial conditions are washed out within a short distance needs to be clarified. Provided that $\rho > 0{\cdot}5$ (the range of insignificant convective inertia), the radial extent of the 'inlet region' is small and its effect on overall flow characteristics, such as the net pressure drop, is negligible. But if $\rho_1 < 0{\cdot}5$ the radial extent of the inlet region may be significant in comparison with the radius of the flow field, though still limited to $\rho_1 < \rho < 0{\cdot}5$ approximately, and its effect on overall flow characteristics must be calculated. We might conjecture that the thin-film approximation is uniformly valid for the prediction of flows with no swirl for all entrance conditions, provided that $\rho_1 \geqslant 0{\cdot}5$. If $\rho_1 < 0{\cdot}5$ then the present solution, or any other solution for that matter,

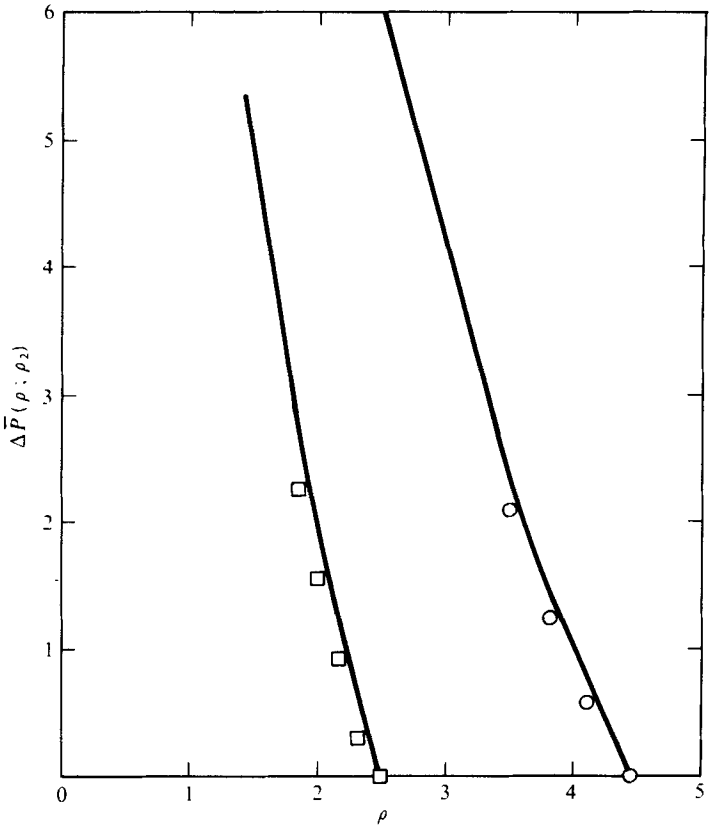

FIGURE 3. $\overline{\Delta P}(\rho;\rho_2)$ *vs.* ρ. Experimental data (Makay 1967): ○, $E = 2{\cdot}73$, $R_Q = 1{\cdot}38\times10^5$, $s = 5{\cdot}08\times10^{-3}$ cm; □. $E = 0{\cdot}93$, $R_Q = 1{\cdot}87\times10^5$, $s = 8{\cdot}64\times10^{-3}$ cm. ——, theory, present authors.

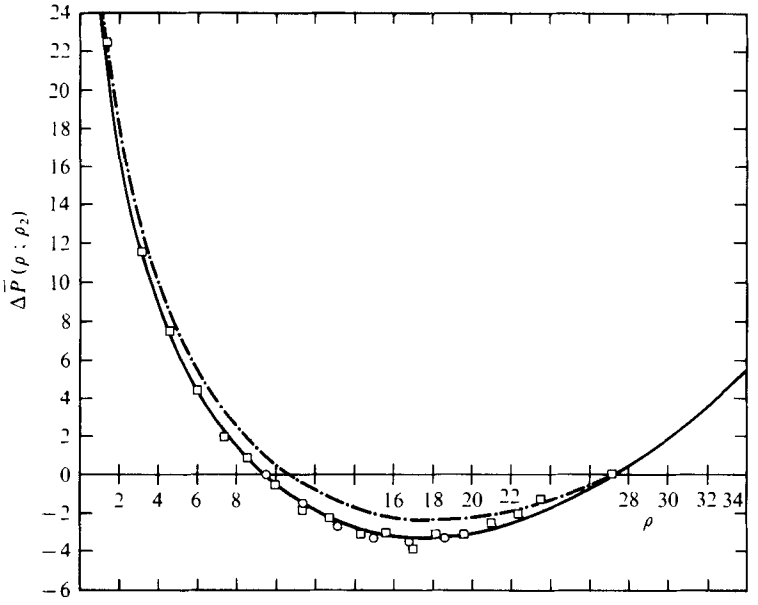

FIGURE 4. $\overline{\Delta P}(\rho;\rho_2)$ *vs.* ρ. Experimental data: □, $E = 2{\cdot}9$, $R_Q = 52{\cdot}11$, $s = 3{\cdot}24\times10^{-2}$ cm (Coombs & Dowson 1965); ○, $E = 2{\cdot}91$, $R_Q = 418{\cdot}4$, $s = 2{\cdot}58\times10^{-2}$ cm (Nirmel 1970). Theory: –·–, Osterle & Hughes (1957/8); ——, present authors.

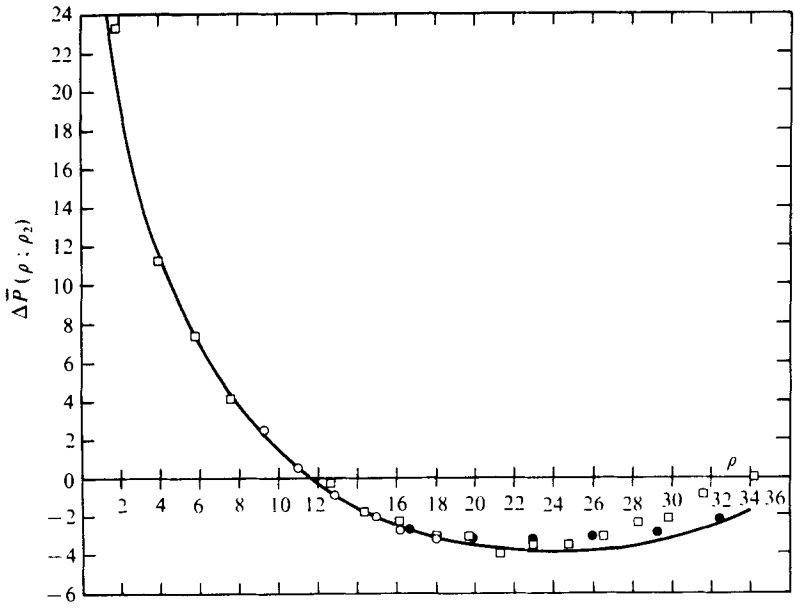

FIGURE 5. $\overline{\Delta P}(\rho;\rho_2)$ *vs.* ρ. Experimental data: □, $E = 3{\cdot}86$, $R_Q = 41{\cdot}0$, $s = 2{\cdot}9\times10^{-2}$ cm (Coombs & Dowson 1965); ○, $E = 3{\cdot}83$, $R_Q = 190{\cdot}7$, $s = 3{\cdot}96\times10^{-2}$ cm; ●, $E = 3{\cdot}85$, $R_Q = 69{\cdot}75$, $s = 3{\cdot}64\times10^{-2}$ cm (Nirmel 1970). ——, theory, present authors.

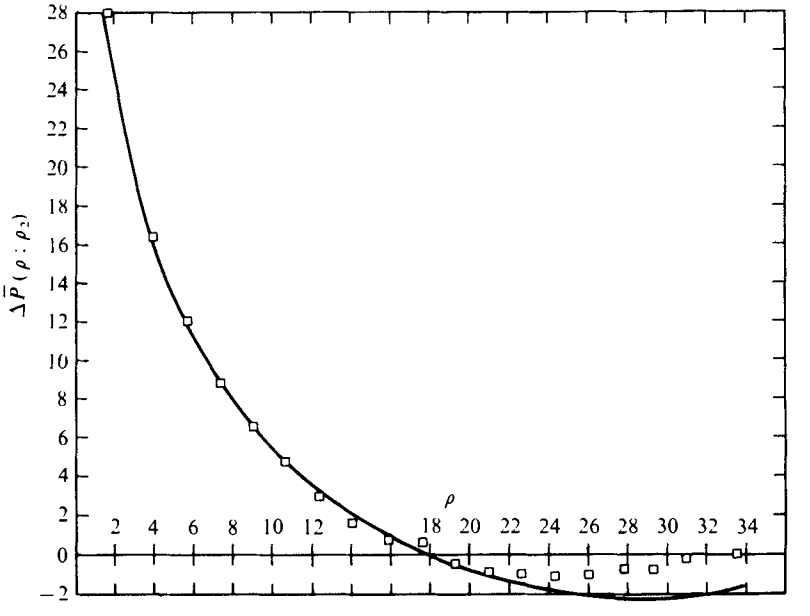

FIGURE 6. $\overline{\Delta P}(\rho;\rho_2)$ *vs.* ρ. □, experimental data, $E = 4{\cdot}89$, $R_Q = 82{\cdot}29$, $s = 2{\cdot}08\times10^{-2}$ cm (Coombs & Dowson 1965); ——, theory, present authors.

E	$\overline{\Delta P}$ (N/m²)	Q (cm³/s)	W (N)
2·9	$2{\cdot}58 \times 10^5$	19·34	$7{\cdot}16 \times 10^3$
(1176 r.p.m.)		(12·13)	$(1{\cdot}43 \times 10^4)$
	$1{\cdot}50 \times 10^6$	77·35	$7{\cdot}50 \times 10^4$
		(69·65)	$(8{\cdot}25 \times 10^4)$
0·932	$1{\cdot}01 \times 10^6$	117·78	$-6{\cdot}96 \times 10^3$
(3660 r.p.m.)		(46·96)	$(5{\cdot}52 \times 10^4)$
	$6{\cdot}28 \times 10^6$	309·06	$2{\cdot}19 \times 10^5$
		(291·53)	$(3{\cdot}45 \times 10^5)$

TABLE 2. Hydrostatic-bearing performance. $r_1 = 5{\cdot}207$ cm; $r_2 = 26{\cdot}035$ cm; $s = 0{\cdot}00508$ cm; $\mu = 9{\cdot}1907 \times 10^{-4}$ N s/m²; $\nu = 9{\cdot}2174 \times 10^{-7}$ m²/s. Numbers in brackets from creeping-flow solution.

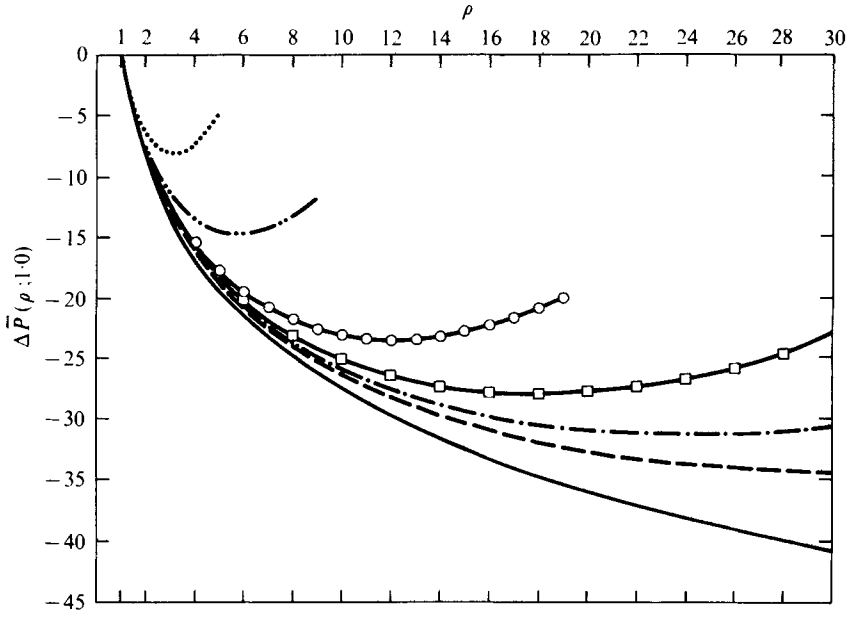

FIGURE 7. $\overline{\Delta P}(\rho; 1{\cdot}0)$ *vs.* ρ. Theory (present authors): ——, creeping flow; – – –, $E = 4{\cdot}89$; –·–, $E = 3{\cdot}86$; –□–, $E = 2{\cdot}9$; –○–, $E = 2{\cdot}0$; –··–, $E = 0{\cdot}932$; ·····, $E = 0{\cdot}5$.

should contain the actual value of ρ_1 together with the actual initial conditions. (A change in the value of the Ekman number does not seem to alter these conclusions.) The experimental data in figure 2 include the ρ range of significant convective inertia and were obtained with $\rho_1 = 0{\cdot}1$. The same value of the inlet radius was used when calculating the two theoretical curves, one by the proposed method and the other from the formula of Jackson & Symmons (1965*b*).

In the second category of experiments one disk is rotated and the other is stationary. For Makay's (1967) data in figure 3, the flow rate is moderately large. In consequence the experimental points fall in the intermediate ρ range where convective inertia has already lost its significance ($\rho > 0{\cdot}5$) while rotational inertia has not yet made its strong effect felt owing to the large values of the Ekman number in the experiments. The data in figure 4 of Coombs & Dowson (1965) and Nirmel (1970) were obtained

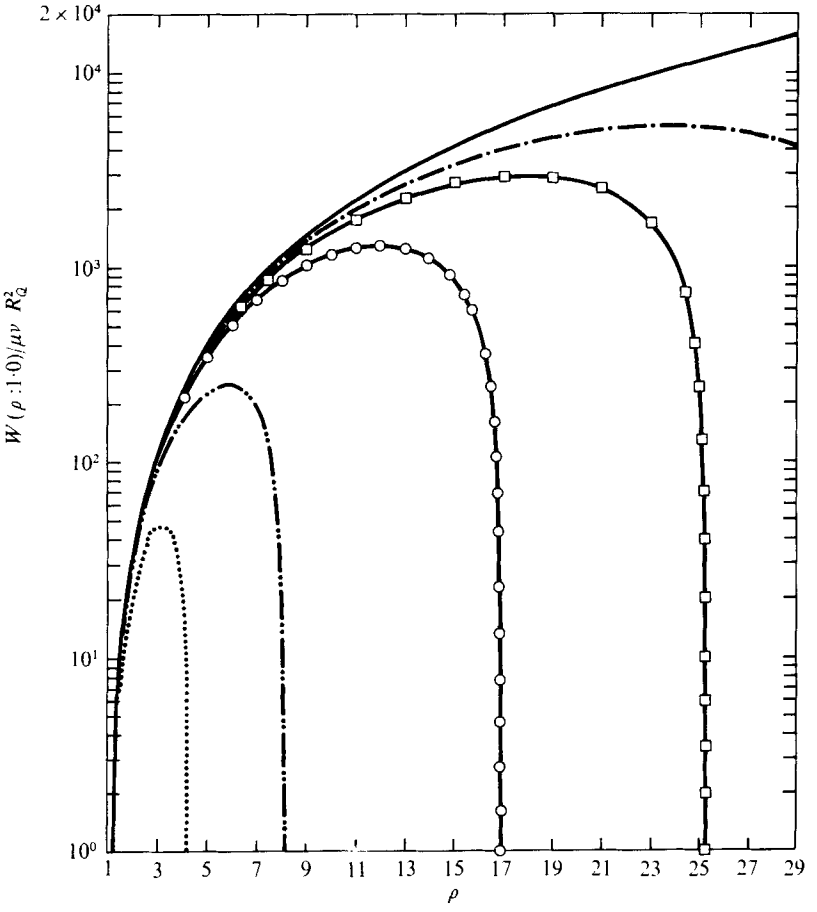

FIGURE 8. $W(\rho, 1{\cdot}0)/\mu\nu R_Q^2$ *vs.* ρ. Theory (present authors): ——, creeping flow; –·–, $E = 3{\cdot}86$; –□–, $E = 2{\cdot}9$; –○–, $E = 2{\cdot}0$; – · · –, $E = 0{\cdot}932$; · · · · ·, $E = 0{\cdot}5$.

at low rates of flow. These data cover a large ρ range, and consequently, even though their Ekman number is comparable to the Ekman number for figure 3, they show very significant rotational-inertia effects. A comparison of figures 4, 5 and 6 indicates that the position of zero radial pressure gradient moves towards the axis of rotation as E is decreased. Then, supposedly, at some small value of E it is possible to have significant rotational effects within the inlet region; we have been unable to find experimental data obtained under such conditions.

On the basis of the foregoing comparison with experimental data we might conclude that the present method underestimates somewhat the effect of rotational inertia (see figure 6 at large ρ), but that in general it offers a satisfactory solution to the problem at hand. In order to judge its capability in predicting convective-inertia effects, however, calculations should be performed using the actual initial conditions of the experiment. (This could be done by simply changing (18*a*, *b*) if the entrance conditions of the experiments were known.) We mention here that all the calculations reported in this paper were made with four Galerkin terms. The reader interested in convergence studies is referred to Adams (1977) and Szeri & Adams (1976).

ρ	$(2E/\pi)\ C_M(\rho; 1{\cdot}0)_R$	$(2E/\pi)\ C_M(\rho; 1{\cdot}0)_S$
1·5	5·3	3·3
2·0	18·3	12·8
2·5	44·1	34·1
3·0	89·3	73·8
4·0	272·9	243·2
5·0	652·8	604·9
6·0	1337·0	1267·0
7·0	2458·0	2362·0

TABLE 3. Torque coefficients at $E = 2{\cdot}9$.

It remains now to indicate the usefulness of the present solution in a quantitative prediction of rotational-inertia effects, say in a thrust bearing. The bearing of our choice has $r_1 = 5{\cdot}207$ cm and $r_2 = 26{\cdot}035$ cm. The thickness of the lubricant film is maintained at $s = 0{\cdot}00508$ cm and the lubricant viscosities are $\mu = 9{\cdot}1907 \times 10^{-4}$ Ns/m^2 and $\nu = 9{\cdot}2174 \times 10^{-7}$ m^2/s. The entries in table 2 were calculated with the aid of figure 7, figure 8 and (26), and pertain to rotational speeds of $N = 1176$ r.p.m. and $N = 3660$ r.p.m. (Table 2 also contains the creeping-flow solution.) At higher recess pressures the predictions of the present theory approach the creeping-flow solution (though our flow rates are higher and our load capacities are lower, consistently). Such is not the case at lower recess pressures. The loss of load capacity is only 50 % relative to creeping flow at the lower speed and lower recess pressure, but at the higher speed and lower recess pressure the load capacity becomes negative. Film collapse could be prevented by increasing the recess pressure, i.e. by moving to the left on the appropriate curve E = constant in figure 7. Figures 7 and 8 were constructed with practical thrust-bearing designs in mind. Typically, for air bearings $E \sim 175$, for water bearings $E \sim 1{\cdot}0$ and for oil bearings $E \sim 2{\cdot}0$. The range of many practical bearings is adequately covered by these figures. Torque calculations show (*a*) that the torque is always smaller on the stationary disk and larger on the rotating disk than that given by the assumption of a linear circumferential velocity (Osterle & Hughes 1957/8) and (*b*) that bowing of the circumferential velocity profile, due to interaction with the throughflow, and the consequent discrepancy between the torques on the two disks are more significant at low values of ρ, as indicated in table 3.

The authors are pleased to express their indebtedness of Prof. D. Dowson of Leeds University for supplying them with details of his experiments and to Prof. W. C. Griffith of North Carolina State University for drawing their attention to the work of C. N. Nirmel. They are also grateful for the reviewers' comments.

Appendix

The notation

$$\langle F \rangle = \pi \int_0^1 F(\zeta)\, d\zeta$$

is used here.

$$A_k^{(1)} = \langle \overline{\phi}' \overline{\phi}'' F_k \rangle, \qquad B_k^{(1)} = \langle \overline{\phi}' \overline{\theta} G_k \rangle,$$

$$A_{kn}^{(2)} = \langle \overline{\phi}'' F_n' F_k' + \overline{\phi}' F_n'' F_k \rangle, \qquad B_k^{(2)} = \langle \overline{\theta} F_n' G_k \rangle,$$

$$A_{knj}^{(3)} = \langle F_k F_n' F_j'' \rangle, \qquad B_{kn}^{(3)} = \langle \overline{\phi} G_n G_k \rangle,$$

$$A_{kn}^{(4)} = \langle \overline{\phi}' F_n'' F_k \rangle, \qquad B_{knj}^{(4)} = \langle F_j' G_n G_k \rangle,$$

$$A_{kn}^{(5)} = \langle \overline{\phi}'' F_n F_k \rangle, \qquad B_{kn}^{(5)} = \langle \overline{\theta}' F_n G_k \rangle,$$

$$A_{knj}^{(6)} = \langle F_k F_n F_j''' \rangle, \qquad B_{knj}^{(6)} = \langle F_j G_n' G_k \rangle,$$

$$A_{kn}^{(7)} = \langle \overline{\theta}' G_n F_k + \overline{\theta} G_n' F_k \rangle, \qquad B_k^{(7)} = \langle \overline{\theta}'' G_k \rangle,$$

$$A_{knj}^{(8)} = \langle G_n G_j' F_k \rangle, \qquad B_{kn}^{(8)} = \langle F_n'' G_k \rangle.$$

$$A_k^{(9)} = \langle \overline{\phi}^{\mathrm{iv}} F_k \rangle,$$

$$A_{kn}^{(10)} = \langle F_n^{\mathrm{iv}} F_k \rangle,$$

$$A_k^{(11)} = \langle \overline{\theta} \overline{\theta}' F_k \rangle,$$

REFERENCES

ADAMS, M. L. 1977 Incompressible flow between finite disks. Ph.D. dissertation, University of Pittsburgh.

COOMBS, J. A. & DOWSON, D. 1965 An experimental investigation of the effects of lubricant inertia in hydrostatic thrust bearings. *Proc. Inst. Mech. Engrs* **179** (3), 96–108.

DOWSON, D. 1961 Inertia effects in hydrostatic thrust bearings. *J. Basic Engng, Trans. A.S.M.E.* **83**, 227–234.

HUNT, J. B. & TORBE, I. 1962 Characteristics of a hydrostatic thrust bearing. *Int. J. Mech. Sci.* **4**, 503–516.

JACKSON, J. D. & SYMMONS, G. R. 1965*a* The pressure distribution in a hydrostatic thrust bearing. *Int. J. Mech. Sci.* **7**, 239–242.

JACKSON, J. D. & SYMMONS, G. R. 1965*b* An investigation of laminar radial flow between two parallel discs. *Appl. Sci. Res.* A **15**, 59–75.

LIVESEY, J. L. 1960 Inertia effects in viscous flows. *Int. J. Mech. Sci.* **1**, 81–88.

MAKAY, E. 1967 Effect of inertia terms on a fully developed axi-symmetric laminar flow. Ph.D. dissertation, The University of Pennsylvania.

MOLLER, P. S. 1963 Radial flow without swirl between parallel discs. *Aero. Quart.* **14**, 163–186.

NIRMEL, C. N. 1970 An analytical and experimental investigation of viscous incompressible flow through narrow regions with and without rotating boundaries. Ph.D. dissertation, North Carolina State University. (Available from University Microfilms, Ann Arbor.)

OSTERLE, J. F. & HUGHES, W. F. 1957/8 Inertia induced cavitation in hydrostatic thrust bearings. *Wear* **4**, 228–233.

SAVAGE, S. B. 1964 Laminar radial flow between parallel plates. *J. Appl. Mech., Trans. A.S.M.E.* **86**, 594–596.

SZERI, A. Z. & ADAMS, M. L. 1976 Source flow between a stationary and a rotating disk. *Mech. Res. Comm.* **3**, 231–232.